HEAT DISSIPATION ENHANCEMENT USING STAGGERED FIN HEAT SINK

By:

ONG ZI HUI

(Matric No.: 142842)

Supervisor:

Dr Yu Kok Hwa

24th July 2022

The dissertation is submitted to
Universiti Sains Malaysia
As partial fulfilment of the requirement to graduate with honours degree in
BACHELOR OF ENGINEERING (MECHANICAL ENGINEERING)

School of Mechanical Engineering
Engineering Campus
Universiti Sains Malaysia

DECLARATION

I hereby declare that this project entitled “Heat Dissipation Enhancement Using Staggered Fin Heat Sink” submitted to Universiti Sains Malaysia is based on my original work except for quotations and citations which have been duly noted by explicit references.

Name: Ong Zi Hui

Date: 24th July 2022

ACKNOWLEDGEMENT

First of all, I would like to express my utmost gratitude to my supervisor, Dr. Yu Kok Hwa for his patience, guidance and enthusiastic encouragement throughout my research progress. He has been extremely supportive in technical issues, where he provided a workstation required for the simulation work as well as offered expert advice on research practices.

I would also like to thank Dr. Muhammad Fauzinizam Bin Razali for organizing seminars to help on my project management and thesis writing. Special dedication to the lecturers and library staff at Universiti Sains Malaysia who provided resources and materials that assisted me in developing and finalizing my thesis.

Finally, I am thankful to my family and friends for their continuous support and understanding when undertaking my research.

TABLE OF CONTENTS

LIST OF TABLES

LIST OF FIGURES

LIST OF SYMBOLS

A	Cross-sectional area of the inlet (m^2)
A_{base}	Area of the base of the heat sink (m^2)
A_T	Total area of heat sink subjected to fluid flow (m^2)
C_p	Specific heat capacity ($Jkg^{-1}K^{-1}$)
D_h	Hydraulic diameter of inlet (m)
$E_{\overline{Nu}}/E_P$	Trade-off between the Nusselt number and pumping power required
$\bar{h}$	Average heat transfer coefficient
k	Thermal conductivity ($Wm^{-1}K^{-1}$)
L	Fin length
$\dot{m}_a$	Mass flow rate of air (kgs^{-1})
$\overline{Nu}$	Average Nusselt number
P	Pressure (Pa)
P_{in}	Inlet pressure (Pa)
P_{out}	Outlet pressure (Pa)
P_{pump}	Pumping power (W)
ΔP	Pressure drop between inlet and outlet (Pa)
P_w	Wetted perimeter of the inlet (m)
q	Heat flux (Wm^{-2})
Q	Heat transfer rate (W)
Re_{Dh}	Reynolds number of air flow at the inlet
R_{th}	Thermal resistance (KW^{-1})
S_L	Longitudinal fin pitch (m)

T	Temperature
T_{avr}	Average air temperature (K)
T_b	Base temperature (K)
T_{in}	Inlet temperature of air (K)
T_{out}	Outlet temperature of air (K)
$\vec{U}$	Velocity (ms^{-1})
U_{avr}	Average velocity of air (ms^{-1})
u	Velocity component in x-direction (ms^{-1})
v	Velocity component in y-direction (ms^{-1})
w	Velocity component in z-direction (ms^{-1})
τ	Viscous stress tensor (Pa)
θ	Angle of fin inclination (°)
μ	Dynamic viscosity $(kgm^{-1}s^{-1})$
ρ	Density (kgm^{-3})
ρ_a	Density of air (kgm^{-3})

ABSTRAK

Kajian ini memberi tumpuan kepada penyelidikan berangka mengenai pelesapan haba dalam sink haba plat sirip (PFHS). Sink haba yang diperbuat daripada aloi aluminium 6061 tertakluk kepada aliran pensantakan dengan nombor Reynolds dalam julat 1333 hingga 5334 pada 25 ℃. Permukaan bawah sink haba tertakluk kepada fluks haba malar 18750 Wm^{-2}. Kajian parametrik dijalankan untuk menyiasat kesan parameter geometri dan aliran ke atas prestasi sink haba. Keputusan menunjukkan bahawa PFHS berperingkat menunjukkan rintangan haba yang lebih rendah dan kuasa pengepaman yang lebih tinggi berbanding dengan PFHS tradisional. Antara sudut kecondongan yang dikaji melibatkan θ = 0˚, 30˚, 60˚, 90˚, 30˚ berselang-seli dan 60˚ berselang-seli, PFHS berperingkat dengan θ = 90˚ menunjukkan peningkatan tertinggi dalam kedua-dua nombor Nusselt dan kuasa pengepaman berbanding dengan PFHS tradisional, manakala θ = 0˚ mempunyai pertukaran terbaik antara nombor Nusselt dan kuasa pengepaman. Konfigurasi selang seli untul θ = 30˚ dan θ = 60˚ menghasilkan prestasi pelesapan haba yang lebih baik berbanding dengan sink haba tanpa seli, walaupun dengan peningkatan kuasa pengepaman yang diperlukan. Selaras dengan peningkatan S_L/L sink haba daripada 0.81 ke 1, rintangan haba menjadi berkurangan manakala kuasa pengepaman yang diperlukan meningkat. Pic sirip membujur tidak mempunyai kesan ketara ke atas pertukaran antara nombor Nusselt dan kuasa pengepaman yang diperlukan untuk sink haba. Berbanding dengan PFHS berperingkat dengan dinding, konfigurasi tanpa dinding menunjukkan rintangan haba yang lebih rendah walaupun purata nombor Nusselt-nya lebih rendah. Konfigurasi tanpa dinding juga menunjukkan kuasa pengepaman yang lebih rendah, serta prestasi pertukaran yang lebih baik antara nombor Nusselt dan kuasa pengepaman.

ABSTRACT

The current study focuses on the computational evaluation of the heat dissipation of staggered plate fin heat sinks (PFHS). The simulation setup consists of an aluminium alloy 6061 heat sink exposed to impinging air flow with Reynolds number in the range of 1333 to 5334 at 25 ℃. A constant heat flux of 18750 Wm^{-2} is applied at the bottom surface of the heat sink. A parametric study is carried out to study the influences of the geometric and flow parameters on the heat sink performance. The results show that the staggered PFHS shows a lower thermal resistance and higher pumping power required as compared with the conventional PFHS. Among the inclination angles studied involving θ = 0˚, 30˚, 60˚, 90˚, alternating 30˚, and alternating 60˚, the staggered PFHS with θ = 90˚ shows the highest increase in both Nusselt number and pumping power required in comparison to the conventional PFHS, whereas configuration with θ = 0˚ yields the best trade-off between Nusselt number and pumping power required. Alternating the θ = 30˚ and θ = 60˚ configurations result in better heat dissipation performance of the heat sink in comparison to that without alternation, albeit with an increase in the pumping power required. As S_L/L increases from 0.81 to 1, the thermal resistance of the heat sink decreases slightly while the pumping power of the heat sink increases. The longitudinal fin pitch of the heat sink has no significant effect on its trade-off between Nusselt number and pumping power required. As compared with the staggered PFHS with wall, the no wall configuration exhibits a slightly lower thermal resistance but a lower average Nusselt number. The no wall configuration shows a lower pumping power required, as well as a better trade-off performance between Nusselt number and pumping power.

CHAPTER 1.

INTRODUCTION

1.1 General Introduction

With the rapid growth of electronics technology, a trend towards miniaturized electronics is gaining momentum, where the sizes of electronic devices and chips are made smaller and their density reduced. These devices produce higher heat fluxes, consequently demanding more advanced thermal management solutions to tackle these issues. Excessive heat accumulation in the electronic device due to the lack of adequate dissipation will lead to performance deterioration, and conceivably permanent failure.

The effective removal of heat from the devices has become a critical issue to ensure safe and dependable device operation. Advancements have been made in cooling technologies to address this topic, such as the implementation of heat pipes, liquid cold plates, immersion cooling and the use of phase change materials (Hasan et al., 2016).

However, heat sink stands firm as the most common heat dissipation device in electronics due to its low cost. The base of a heat sink is attached to the surface of a heat source i.e. electronic chip. The primary purpose of this heat sink is to enlarge the surface area of the electronic component by the use of fins and thus create an efficient heat dissipation route from the hot device into the heat sink and then into the environment. Heat transfer occurs in three modes, heat conduction from the electronic chip to the heat sink, and subsequently, heat convection as well as radiation from the heat sink to the ambient air (Mjallal et al., n.d.).

Heat sinks are usually made of metals with high thermal conductivity such as aluminium or copper. Although copper has a thermal conductivity about 70% higher

than that of aluminium (Ansari & Jeong, 2020), significant cost and weight savings can be achieved with the choice of aluminium heat sinks. However, there is a drawback to both aluminium and copper materials, that is they both suffer from high coefficient of thermal expansion. Nowadays, new materials such as graphene, a 2-D allotrope of carbon, is studied for the fabrication of heat sink. Graphene integrates high thermal conductivity and low thermal expansion, and also possesses excellent mechanical strength (El-Kady et al., 2019).

Porous materials, such as metal foams, also provide a promising material alternative in applications requiring high heat transfer rates (Rehman & Ali, 2019). Monolithic carbonaceous materials show potential in thermal management applications, including liquid-to-liquid heat exchangers, liquid-to-gas heat exchangers, gas-to-gas heat exchangers, and heat sinks (Wang et al., 2012).

The most common heat sinks currently available in the market are the plate fin heat sink and pin fin heat sink. Plate fin heat sink is more extensively used on account of its simple design and ease of manufacturing. On the other hand, pin fin heat sink has a higher heat transfer performance than plate fin, but comes with a cost of pressure drop. Yamac and Koca (2018) conducted a study where the outcome revealed that pin fin heat sink has 40% less thermal resistance than plate fin heat sink at a constant surface area. Kim et al. (2010) further discovered that the thermal resistance for optimized plate fin heat sink is lower than that for optimized pin fin heat sink at small dimensionless pumping powers and large dimensionless heat sink lengths, and vice versa.

The result of the geometry combination of the two heat sinks mentioned above is the plate-pin fin heat sink, which consists of pins staggered between plate fins.

Numerical simulations and experiments conducted by Yu et al. (2005) showed that plate-pin fin heat sink exhibited 30% less thermal resistance at constant wind velocity.

Heat sinks are also available in various configurations, such as different shapes of pin-fin cross section as well as inline or staggered arrangements. Plate fins can either be continuous (parallel plates) or staggered, while pin fins can either be inline or staggered (Muhammad, 2013).

In the staggered arrangement, the fins are arranged in a zigzag manner. Although the inline arrangement has more fins packed together and thus a larger convection surface area, the staggered arrangement demonstrated a superior heat transfer performance because of the relatively narrow fin spacing of the inline arrangement, consequently leading to reduction of entrance flow rate (Yeh et al., 2007). Additionally, vortex formation and higher turbulence due to the staggered arrangement of fins results in a significant increase in cooling rate (Sakib & Al-Faruk, 2018).

1.2 Project Background

All electronic devices are affected by excessive heat during operating, and with the devices becoming denser and compact, the dissipation of the excess heat becomes more critical than ever. In miniaturized electronic systems, heat sink is often implemented for electronic cooling. A heat sink plays its role in thermal management by increasing the working surface area of the electronic device, such that more heat is transferred away when a fluid flows across its enlarged surface area.

The innovation of heat sink technology has been continuously ongoing in recent years to keep up with the endless quest of packing more processing power into smaller form factors of the electronic devices. Numerous designs of heat sinks with different fin shapes, materials, and dimensions have been studied to enhance the heat removal rate, ultimately to maintain the devices within their operating temperature limits and maximize their longevity.

Typically, heat sinks can be classified according to the fin arrangement, i.e., inline heat sink and staggered heat sink. Generally, the inline configuration shows poorer heat transfer performance as compared with the staggered configuration. This is due to the fact that the staggered array of fins induce distortion to the flow and temperature boundary layers. The increase in turbulence intensity therefore enhances the heat dissipation.

The heat transfer performance of the staggered heat sink gives it an edge over the inline heat sink. Previous researchers have conducted studies to investigate various geometric parameters (fin shape, fin diameter, pitch between adjacent fins, inclination of fins etc.) and flow parameters (flow direction and Reynolds number) for staggered heat sink performance. Optimization process of heat sink design are proposed using

different techniques, all with the objective to further optimize the heat transfer in the heat sink.

Continuous efforts are made perseveringly to discover greater potential of staggered heat sinks in the electronic cooling applications, hence the aligned interest and significance with the purpose of this study.

1.3 Problem Statement

This study will focus on heat sinks with staggered fins that have the capability to significantly enhance the heat transfer performance for the refinement of thermal management in electronic applications. With the rapid development of miniaturized microprocessors, the temperatures of the dense electronic package have also increased substantially. Hence, in order to reduce the temperature of this package, the heat dissipated needs to be further increased.

Staggered fin heat sink shows promising potential in creating a connective transport of thermal energy due to its ability to form larger eddies and vortices for a balanced turbulence mixing of fluid. To the author's best knowledge, the performance of rectangular strip fins at various inclinations for impinging flow are yet to be fully understood, as there have been significantly lesser studies of impinging air flow on staggered PFHSs.

Thus, this research will investigate the flow and heat transfer performance of staggered PFHSs subjected to impinging flow with varying geometric and flow parameters i.e. fin inclination, longitudinal fin pitch, presence of side wall and air mass flow rate.

1.4 Project Objectives

The objectives of this project are summarized as follows:

(i) To investigate the influence of staggered arrangement of fins on the thermal and hydraulic performance of PFHS

(ii) To investigate the influence of fin inclination on the thermal and hydraulic performance of staggered PFHS

(iii) To investigate the influence of longitudinal fin pitch on the thermal and hydraulic performance of staggered PFHS

(iv) To investigate the effect of presence of side wall on the thermal and hydraulic performance of staggered PFHS

1.5 Scope of Research

This study will be pivoted on the numerical simulation of heat dissipation in staggered PFHS using the ANSYS FLUENT software. The conjugate heat transfer of the heat sink is simulated using the finite volume method. The heat sink consists of rectangular strip fins arranged in staggered configuration and is made of aluminium alloy 6061. The heat sink is subjected to impinging air flow, where the flow is assumed to be steady, turbulent and incompressible. Radiation and gravitational acceleration effects are neglected. The performance of the staggered PFHS are compared with that of the conventional PFHS. Fin arrangement with different inclination angles involving $\theta = 0^{\circ}, 30^{\circ}, 60^{\circ}, 90^{\circ}$, alternating 30° and alternating 60° are studied. The influences of longitudinal fin pitch involving S_L/L = 1, 0.94, 0.88 and 0.81, as well as the presence of side wall and air mass flow rate on the thermal and hydraulic performance of the heat

sink are also investigated. The performance evaluation is conducted based on the thermal resistance of the heat sink, pressure drop, as well as average Nusselt number.

1.6 Thesis Outline

The structure of this thesis is as follows:

Chapter 1 provides a general introduction regarding the problems of the thermal management of electronic devices and the potential of staggered fin heat sinks in heat dissipation.

Chapter 2 discusses the literature review of current heat sink research by the scientific community.

Chapter 3 describes the methodology implemented during the numerical simulation of this research in details.

Chapter 4 discusses the results obtained from the works of numerical simulation.

Chapter 5 includes a conclusion of the overall research and recommendations for future work.

CHAPTER 2.

LITERATURE REVIEW

The studies on the heat sink are constantly aimed at the techniques to improve the existing technologies for heat dissipation. Several studies have been conducted on inline and staggered fin heat sinks with various fin cross-sections. Yang et al. (2007) studied experimentally the heat transfer performance for pin fin heat sinks with circular, elliptic and square cross-section. Results showed that the circular pin fin in inline arrangement showed a prominent Coanda effect, where the deflection flow changes the vortex structure behind the fins and causes an improved mixing and heat transfer performance. Heat transfer coefficient increases with a rise in fin density for all three cross-sections with staggered arrangement. The deflection flow effect is eliminated in the staggered configuration as the subsequent row divided the gap flow into separate streams.

Oswal et al. (2007) investigated the thermal performance of fins using ANSYS Icepak. Elliptical and circular pin fins show better heat transfer performance for staggered and inline arrangement respectively. Heat transfer increases with the increase in air velocity, number of pins and Reynolds number. Sahin and Demir (2008a; 2008b)investigated the influence of circular and square cross-section for inline pin arrangement while Dhumme and Farkade (n.d.) studied the effect of staggered pin arrangement for perforated circular cross-section pins. Choudhary et al. (2019) presented a study on the heat transfer performance of pin fin heat sink with and without wings and observed that the addition of wings resulted in improved heat transfer albeit with a moderate increase in frictional losses.

Referring to Figure 2.1, Al-Sallami et al. (2016) studied the thermal and hydraulic performance of inline and staggered arrangements of strip fins, circular pins and square pins, as well as the benefits when perforations are employed. Results indicated that perforations are advantageous for staggered configuration as they help in the reduction of high pressure drop caused by the blockage effect of staggered fins. Strip fins are shown to be significantly effective in disrupting the boundary layer to increase turbulence as well as enhance heat transfer, albeit with high pressure losses.

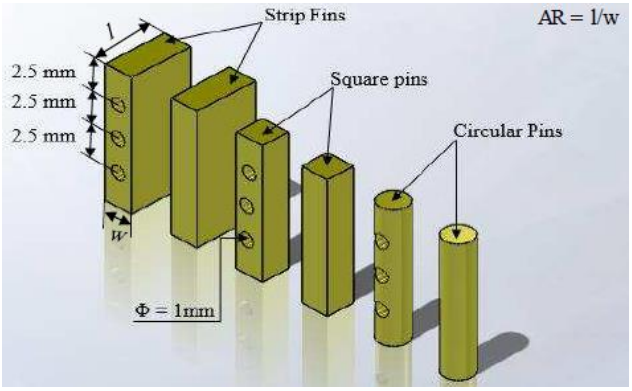

Figure 2.1 The six fin designs considered in the study, and a definition of pin aspect ratio, AR=1/w (Al-Sallami et al., 2016)

Referring to Figure 2.2, Tariq et al. (2021) studied the effect of longitudinal perforations on the thermal and hydraulic performance of plate fin heat sinks. As compared with the conventional plate fin heat sink, the slots and perforations in the proposed heat sink help in reducing the mass of the heat sink, as well as increasing the heat transfer coefficient due to its relatively high surface area.

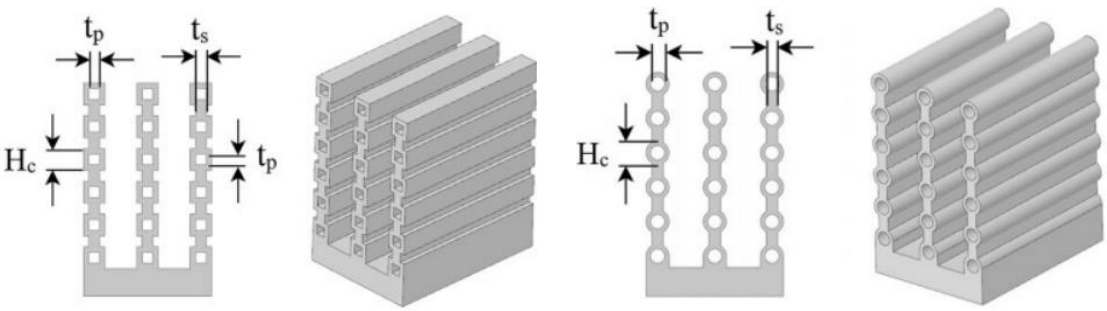

Figure 2.2 Proposed plate fin heat sink with slots and perforations (Tariq et al., 2021)

Zeng et al. (2021) proposed a unique microchannel heat sink with open-ring pin fins design as shown in Figure 2.3 to dissipate heat in devices with high heat flux. Results from experimental and numerical studies show that the inline and staggered open-ring pin fins induced a Nusselt number enhancement of 56 – 220% and 77 – 260%, respectively, in comparison to conventional rectangular microchannels. The open-ring design creates flow mixing and redevelopment of boundary layers, leading to a reduction in thermal resistance as well as a gain in heat transfer. The staggered open-ring pin fin microchannels demonstrated a 6 – 35% improved heat transfer performance, albeit with a 9 – 27% higher pressure drop compared to the inline arrangement.

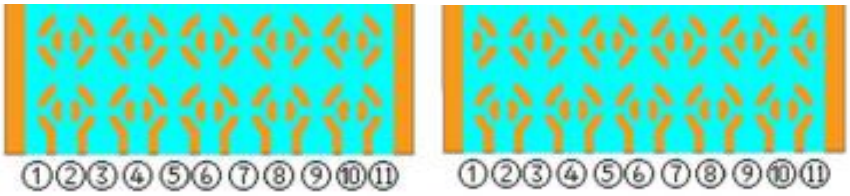

Figure 2.3 Schematic of a section of the microchannels with open-ring pin fins: inline (left) and staggered (right) open-ring pin fins (Zeng et al., 2021)

Effendi et al. (2018) developed a design of hollow hybrid fin heat sink as illustrated in Figure 2.4. Parametric effects due to the fin wall thickness and fin height on the natural convection heat transfer of the heat sink are also discussed in the numerical study.

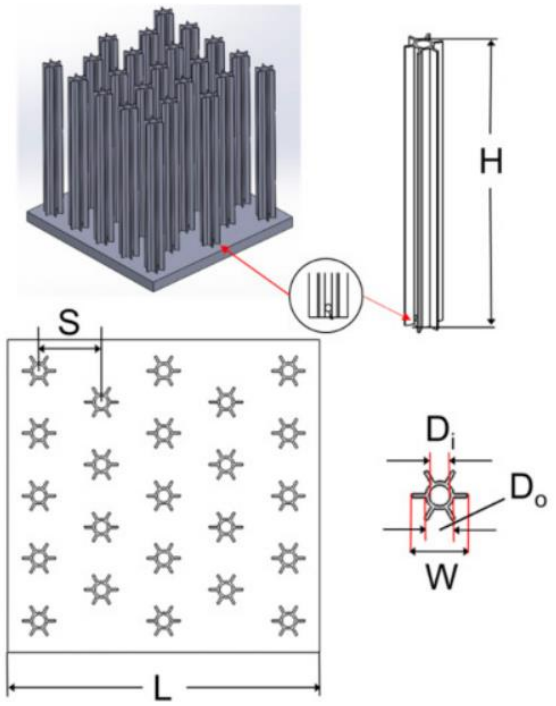

Figure 2.4 The structure of a hollow hybrid fin heat sink (Effendi et al., 2018)

Referring to Figure 2.5, Nilpueng et al. (2021) conducted test runs at a heat flux of 14.81 kWm^{-2} and Reynolds number ranging from 1700 to 5200 to investigate the effect of pin fin configuration on the thermal performance of plate-pin fin heat sinks. Flow visualization is achieved using smoke to observe the air flow pattern in plate-pin fin heat sinks with the circular pin, square pin and 45˚ square pin. With the same fin length, fin pitch and fin frontal area, the heat transfer coefficient and pressure drop of air inside the plate-45˚ square pin fin heat sink was the highest among the three pin cross-sections, i.e. 13.09% and 54.81% higher than the plate-square pin fin heat sink.

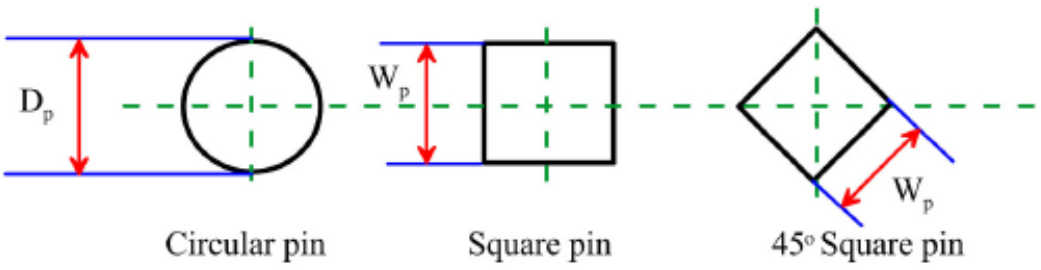

Figure 2.5 Three different pin fin shapes for plate-pin fin heat sinks in this study (Nilpueng et al., 2021)

Khudhur et al. (2022) proposed the design of heat sinks with add and subtract fins as illustrated in Figure 2.6 and Figure 2.7 for a numerical study with Reynolds number in the range of 6300 to 35120. The results are validated with experiments and showed an increase of Nusselt number at approximately 21% and 32% for straight with added and subtracted semi-circular plate fin heat sinks respectively.

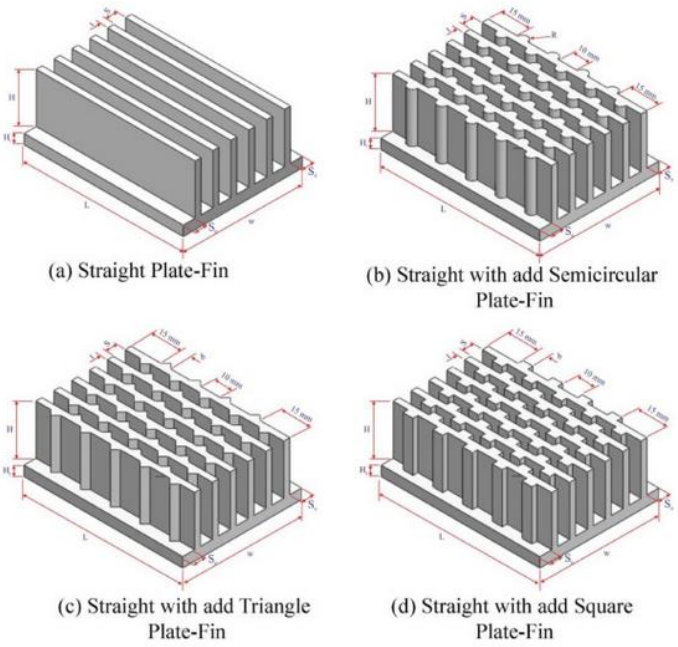

Figure 2.6 Geometric models of straight with add-fin heat sinks (Khudhur et al., 2022)

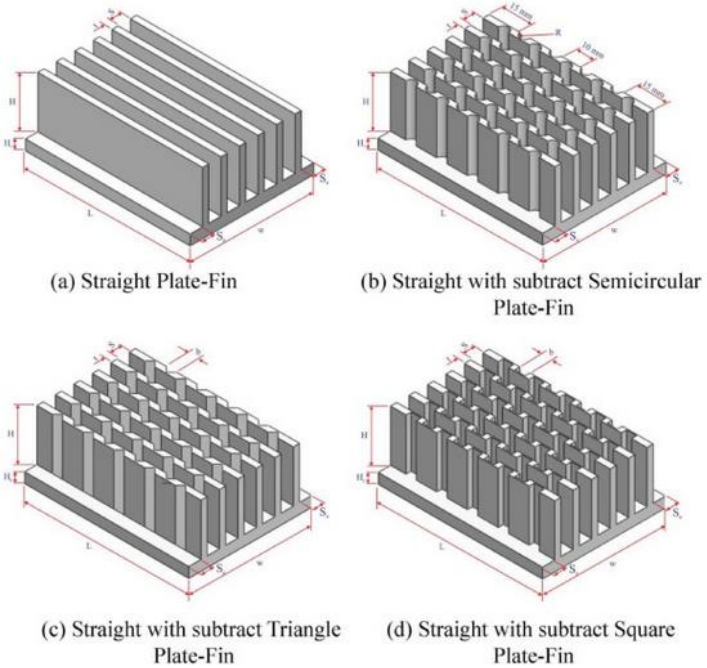

Figure 2.7 Geometric models of straight with subtract-fin heat sinks (Khudhur et al., 2022)

The heat transfer performance is also affected by the location of fan or the direction of air flow with respect to the heat sink. Abdelmohimen et al. (n.d.) executed a numerical analysis on plate fin heat sinks with multiple slides arranged in staggered arrangement. The performance is evaluated in terms of heat sink effectiveness, thermal resistance, pressure drop, pumping power, and Nusselt number for impinging and parallel flow directions from Reynolds number of 1333 to 5334. Parallel flow shows a lower thermal resistance than impinging flow. However, using three slides with impinging flow still shows an admissible diminishment in thermal resistance with minimal change in pumping power.

Hussain et al. (2019) performed a numerical investigation for the impact of flow direction and fillet profile on heat transfer enhancement in plate fin heat sinks. A plate fin heat sink with fillet profile subjected to parallel flow is developed and proven to exhibit lower base temperature and thermal resistance as compared with its alternative (without fillet profile subjected to impinging flow). The fillet profile plays its role by increasing heat transfer area and improving heat distribution by smoothening convection near the base of plate fin.

Duan et al. (2020) further compared the flow characteristics and pressure drop for plate fin heat sinks with or without elliptic bottom profiles. A higher pressure drop occurs for the impinging plate fin heat sink without elliptic bottom profiles at the same inlet width and velocity.

Kim et al. (2009) performed an analysis experimentally and numerically on plate fin and pin fin heat sinks exposed to impinging flow. A volume averaging model is proposed to optimize plate fin and pin fin heat sinks under constant pumping power conditions. Optimized pin fin heat sinks possess lower thermal resistances than

optimized plate fin heat sinks at a small dimensionless pumping power and large dimensionless heat sink length, and vice versa.

Duan and Muzychka (2004) predicted the heat transfer coefficient of plate fin heat sinks subjected to impingement cooling using a semi-empirical model. Thermal resistance decreases while pressure drop across the heat sink increases when the impingement inlet width is reduced at a constant flow rate.

As illustrated in Figure 2.8, Xie et al. (2021) implemented the finite volume method to analyse the thermal and hydraulic performance of microchannel heat sink with pin fins arranged in an inline and staggered pattern and inclined at an angle of 0˚, 30˚, 45˚ and 60˚. The change in friction factor and Nusselt number with the increase of inclined angle does not exhibit a consistent pattern. It is concluded that the arrangement of pin fins has less significant influence in comparison to the angle of inclination, particularly in Reynolds number range of 100 to 300.

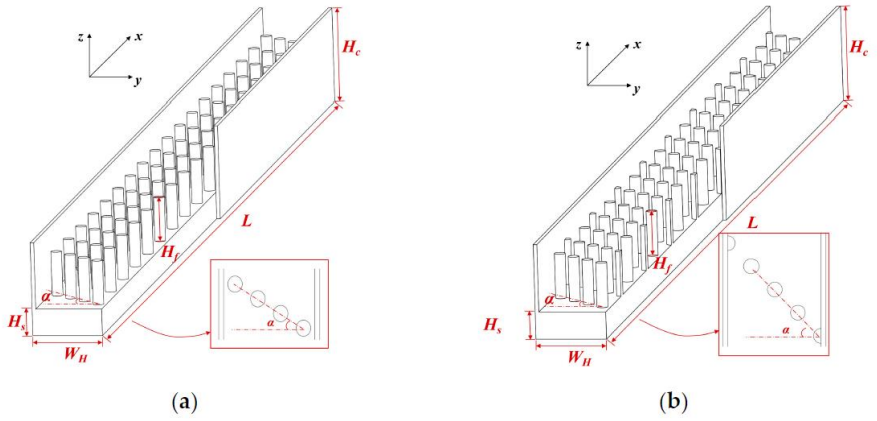

Figure 2.8 The structure of the investigated micro pin fin heat sink with: (a) inline pin fins; (b) staggered pin fins (Xie et al., 2021)

Patil and Dingare (2019) implemented an analysis of the experimental and numerical test of forced convection on plate fin heat sink with rectangular plates at various inclinations with respect to the direction of parallel flow. The heat input supply ranges from 50 W, 80 W, 100 W and 125 W; Reynolds number ranges from 4000 to

18000; and the fin inclination ranges from 0˚, 30˚ and 60˚ for both inline and staggered arrangements. They concluded that the heat transfer coefficient is higher at 30˚ for inline and 0˚ for staggered, both at the edge of introduction of the fins.

Referring to Figure 2.9, Tang et al. (2022) investigated the enhancement of heat transfer with the use of discontinuous staggered ring ribs when impingement flow is implemented. The novel design proved to be advantageous in the formation of secondary flow, thereby leading to a more uniform temperature of the whole heat sink.

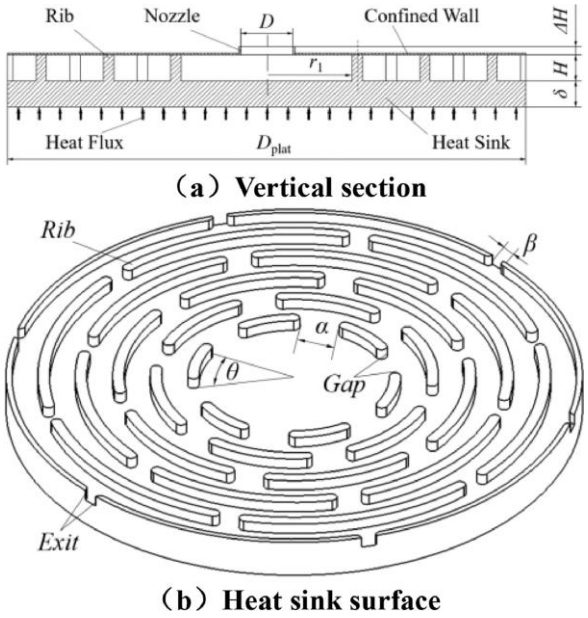

Figure 2.9 Schematic diagram of the ring-ribbed heat sink (Tang et al., 2022)

Wang et al. (2019) conducted an experimental investigation on finned copper foam heat sinks that are subjected to impingement flow. The copper foams inserted in between the aluminium fins proved to enhance the thermal performance of heat sink. However, these resulted in higher flow resistance and pressure drop as compared to those of the conventional finned heat sinks.

Regarding the arrangement of fins, Mousavi et al. (2018) performed a 3D simulation on the heat dissipation from interrupted, staggered and capped fin heat sinks by natural convection and radiation. Air velocity drops as fin spacing decreases for

staggered fins. However, staggering the fins disturbs the boundary layer which may enhance the rate of heat transfer. Results showed that longitudinal pitch less than 3 mm does not improve cooling performance in staggered configuration.

Yadav and Pandey (n.d.) presented a numerical study of inline and staggered micro fin heat sinks with Reynolds number varying from 100 to 900. Nusselt number increases along with Reynolds number, indicating that a higher fluid velocity can increase heat transfer. With heat flux of 100 Wcm^{-2} at the base, results showed that staggered fin heat sink has higher heat transfer rate due to higher turbulence. However, its pressure loss becomes significant for Reynolds number above 450, therefore requiring higher pumping power.

Feng et al. (2018) developed a cross-fin heat sink design as shown in Figure 2.10. The investigation is carried out numerically considering both natural convection and radiation, and experiments are then conducted for validation. Results showed that the overall heat transfer is increased by 11% compared to the conventional plate fin heat sink.

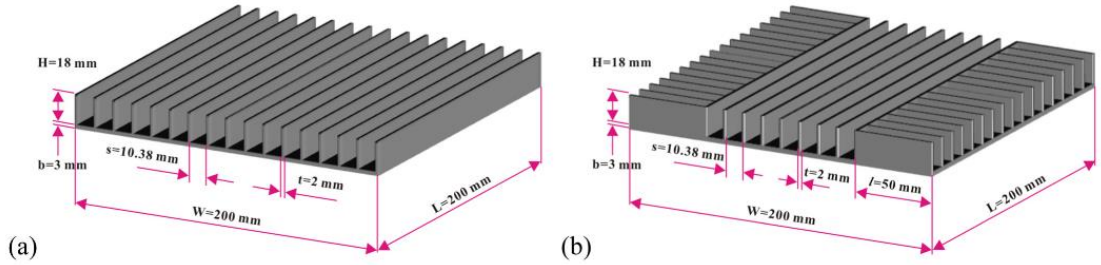

Figure 2.10 Schematic of (a) conventional plate fin heat sink and (b) cross fin heat sink (Feng et al., 2018)

Zhang et al. (2021) proposed that the installation angle of inclined interrupted fins heat sink has a significant effect on its heat transfer performance under natural convection. It was also found that there is an improvement in heat transfer at increased fin heights when the input power is constant.

A numerical analysis on slant rectangular ribs in a microchannel heat sink at Reynolds number of 62.5 to 625 is conducted by Wang et al. (2018) The slanted design disturbs the flow and interrupts the boundary layer, thereby promoting heat transfer. The presence of slant rectangular ribs at both the top and bottom walls of channel as illustrated in Figure 2.11 allows the generation of a stable vortex pair at a higher attack angle and Reynolds number.

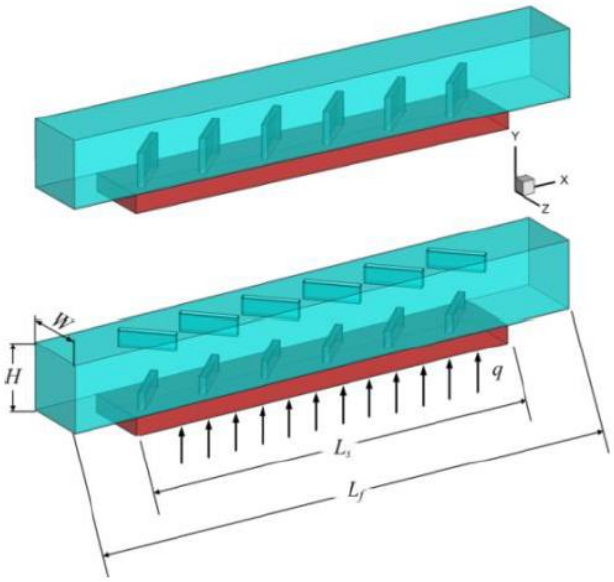

Figure 2.11 Geometry of microchannel heat sink with slant rectangular ribs at: (top) the bottom; (bottom) the top and bottom of the channel (Wang et al., 2018)

Shyu and Jheng (2020) studied the heat transfer enhancement due to plate fin heat sinks featuring winglet vortex generators experimentally and numerically. They discovered that the swept delta winglet pair configuration as shown in Figure 2.12 exhibits the highest thermal enhancement factor of 1.28 at Reynolds number of 1000.

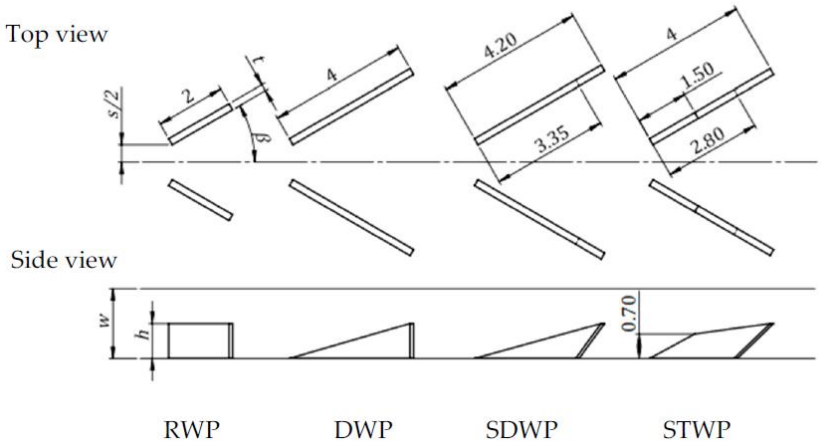

Figure 2.12 Types of tested winglet vortex generators: (left to right) rectangular winglet pair, delta winglet pair, swept delta winglet pair and swept trapezoid winglet pair (Shyu & Jheng, 2020)

Besides, Rezaee et al. (2019) varied the pin length and longitudinal pitch of a pin fin heat sink to investigate the enhancement in heat transfer experimentally and numerically. Referring to Figure 2.13, the results showed that the greatest intensification in heat transfer is achieved when the pin fins have a larger pin length at the entrance flow region and a shorter longitudinal pitch at the exit flow region.

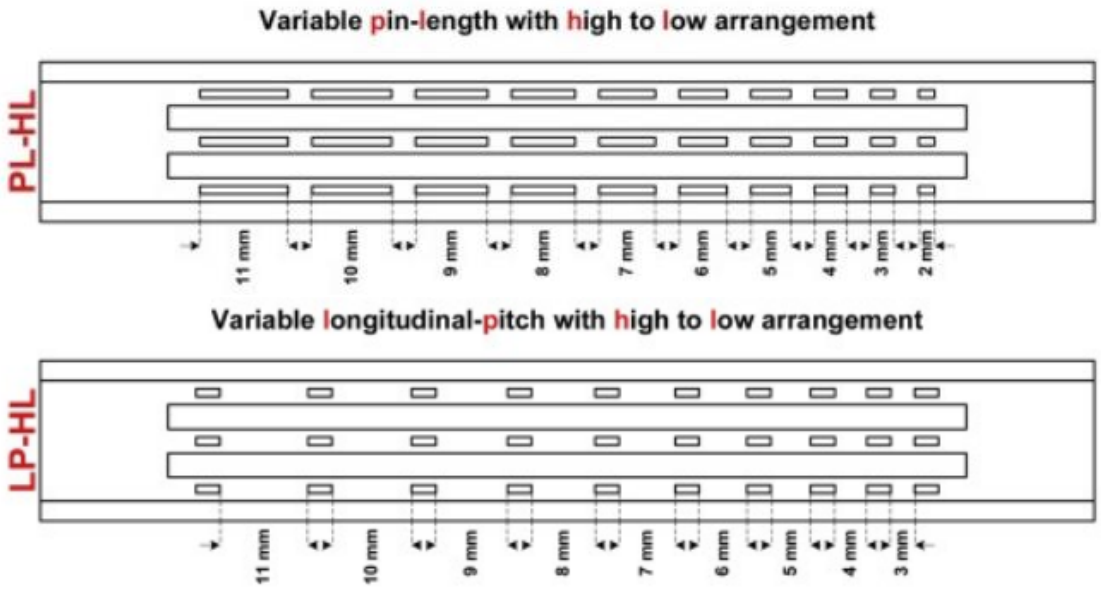

Figure 2.13 Pin fin heat sink configuration with the highest heat transfer enhancement (Rezaee et al., 2019)

CHAPTER 3.

METHODOLOGY

3.1 Model Geometry Description

In this study, the heat transfer performance of a plate fin heat sink (PFHS) in staggered arrangement is studied and compared with that of a conventional PFHS. The geometry of the conventional PFHS is modelled according to the dimensions stated by Abdelmohimen et al. (n.d.) as illustrated in Figure 3.1. The length and width of the base of heat sink are 40 mm and 39.7 mm respectively, with a thickness of 5 mm. The thickness of the fins and channel width are constant across the base length, and are specified as 1 mm and 3.3 mm respectively. The height of the fins is 20 mm without considering the thickness of the base.

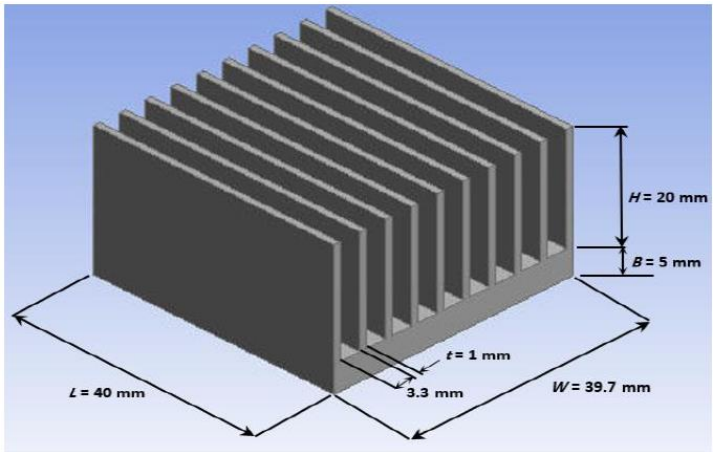

Figure 3.1 Conventional heat sink (Abdelmohimen et al., n.d.)

The staggered PFHS has the same geometric volume as that of the conventional PFHS, as well as the same base dimensions, fin height and fin thickness. The fins are divided into segments of 4 mm length (L) which are then separated with a perpendicular distance of 1.08 mm from the initial centreline of the fin in the conventional PFHS. The transverse and longitudinal pitch values are 2.15 mm and 4 mm respectively. Different heat sink configurations with geometric parameters studied are as illustrated in Figure 3.3. Note that the transverse fin pitch for the staggered PFHS with no wall is 2.04 mm.

The heat sink is situated in the centre of a rectangular fluid domain of length 1m and cross-section of 39.7 mm × 26 mm as shown in Figure 3.2. Impingement flow direction is studied, with one inlet and two outlets on each end of the rectangular fluid domain. Air enters from the inlet, impinges on the heat sink along the y-axis, then exits towards the two outlets along the z-axis.

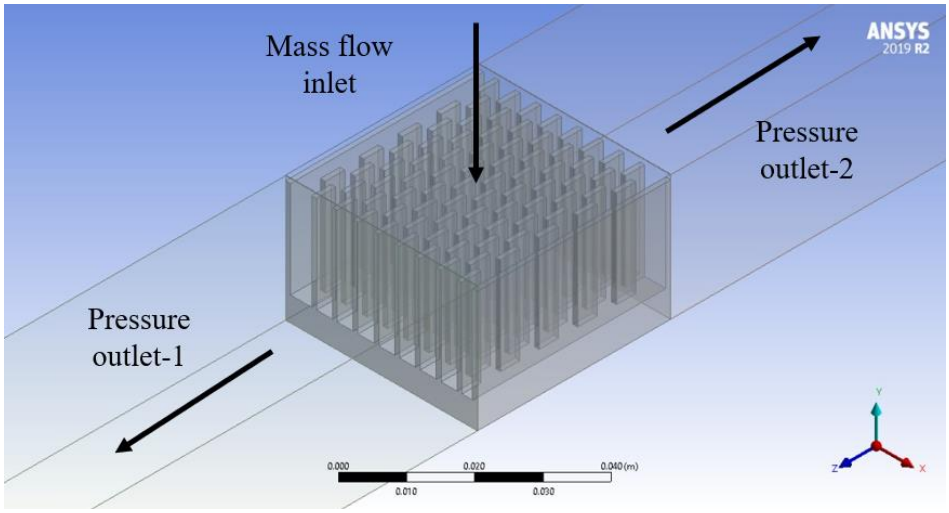

Figure 3.2 Fluid domain of PFHS

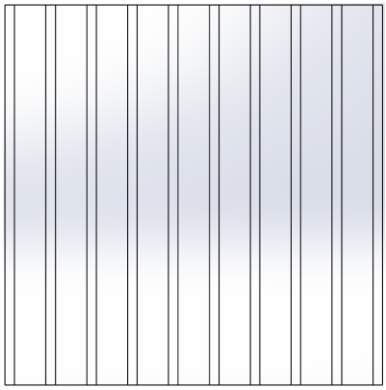

Conventional PFHS

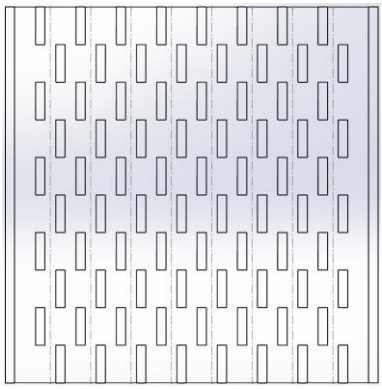

Staggered PFHS with wall, θ = 0˚, S_L/L = 1

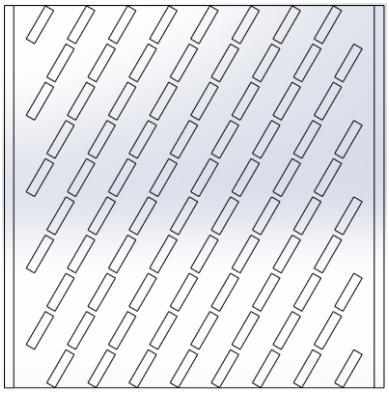

Staggered PFHS with wall, θ = 30˚, S_L/L = 1

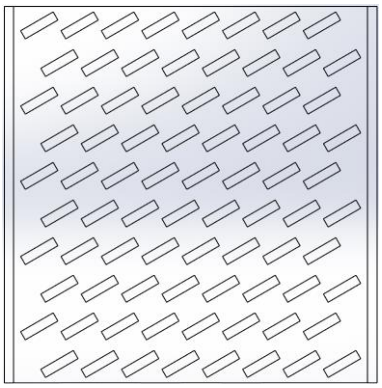

Staggered PFHS with wall, θ = 60˚, S_L/L = 1

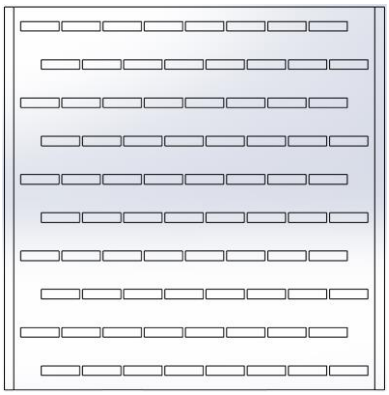

Staggered PFHS with wall, θ = 90˚, S_L/L = 1

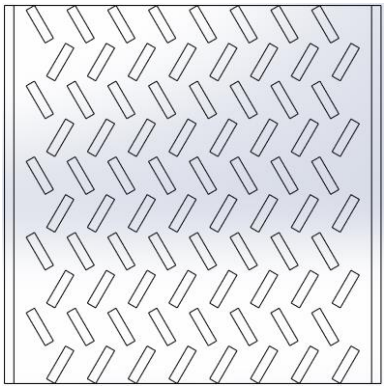

Staggered PFHS with wall, θ = alternating 30˚, S_L/L = 1

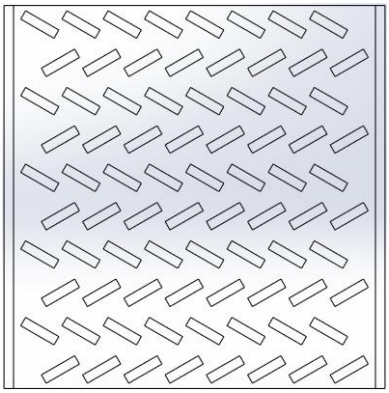

Staggered PFHS with wall,
θ = alternating 60˚, S_L/L = 1

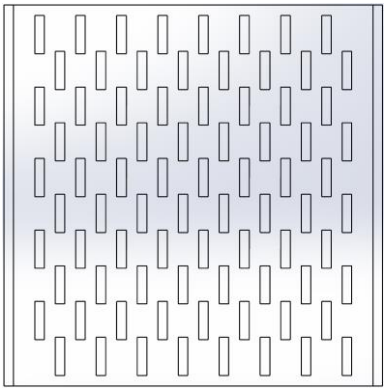

Staggered PFHS with wall,
θ = 0˚, S_L/L = 0.94

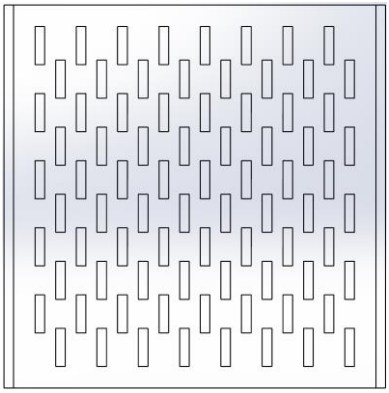

Staggered PFHS with wall,
θ = 0˚, S_L/L = 0.88

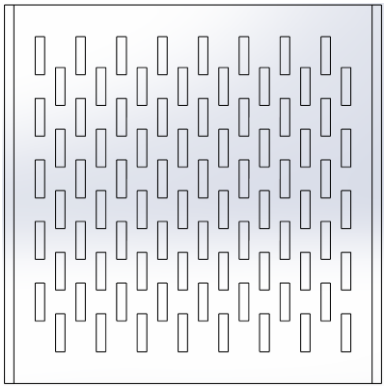

Staggered PFHS with wall,
θ = 0˚, S_L/L = 0.81

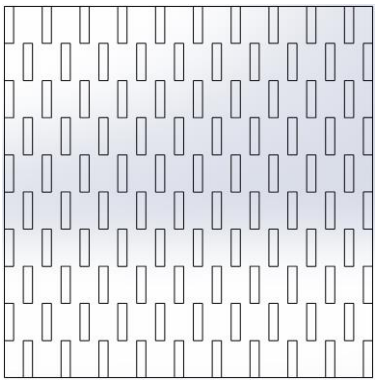

Staggered PFHS with no wall, θ = 0˚, S_L/L = 1

Figure 3.3 Different heat sink configurations for PFHS

3.2 Numerical Methods

3.2.1 Governing Equations

The simulations are set up in ANSYS Fluent 2019 R2 and several assumptions are made in the simulation.

(i) The air flow is steady, turbulent and incompressible.

(ii) Three-dimensional fluid-solid conjugate.

(iii) Effect of gravity acceleration is neglected.

(iv) Radiation effect is neglected.

(v) Energy is conserved.

(vi) The thermophysical properties of air and aluminium alloy 6061 are as shown in Table 3.1.

Table 3.1 Thermophysical properties of working fluid and heat sink material

Materials	Density, $\rho\ (kgm^{-3})$	Specific heat capacity, $C_p(Jkg^{-1}K^{-1})$	Thermal conductivity, $k\ (Wm^{-1}K^{-1})$	Dynamic viscosity, $\mu(kgm^{-1}s^{-1})$
Air	1.1774	1005.7	0.02624	1.8462×10^{-5}
Aluminium alloy 6061	2700	897	171	–

The convective heat transfer characteristics are achieved by solving the governing equations as follows:

3.2.1 (a) Continuity Equation

The continuity equation is given by

$$\nabla \cdot (\rho \vec{U}) = 0 \tag{3.1}$$

where ρ is the density of air and $\vec{U}$ is the velocity of air.

3.2.1 (b) Momentum Equation

The Navier-Stokes equations across the x, y and z directions are given by

$$\nabla(\rho\vec{U}u) = -\frac{\partial P}{\partial x} + \frac{\partial \tau_{xx}}{\partial x} + \frac{\partial \tau_{yx}}{\partial y} + \frac{\partial \tau_{zx}}{\partial z} \tag{3.2}$$

$$\nabla(\rho\vec{U}v) = -\frac{\partial P}{\partial y} + \frac{\partial \tau_{xy}}{\partial x} + \frac{\partial \tau_{yy}}{\partial y} + \frac{\partial \tau_{zy}}{\partial z} \tag{3.3}$$

$$\nabla(\rho\vec{U}w) = -\frac{\partial P}{\partial z} + \frac{\partial \tau_{xz}}{\partial x} + \frac{\partial \tau_{yz}}{\partial y} + \frac{\partial \tau_{zz}}{\partial z} \tag{3.4}$$

where u, v and w are the velocity components in the x, y and z direction, respectively, P is the pressure and τ is the viscous stress tensor.

3.2.1 (c) Energy Equation

The energy equation is given by

$$\rho C_p(u\frac{\partial T}{\partial x} + v\frac{\partial T}{\partial y} + w\frac{\partial T}{\partial z}) = k(u\frac{\partial^2 T}{\partial x^2} + v\frac{\partial^2 T}{\partial y^2} + w\frac{\partial^2 T}{\partial z^2}) \tag{3.5}$$

where C_p is the specific heat capacity of air, k is the thermal conductivity of air and T is the temperature of air.

3.2.2 Simulation Setup

The boundary conditions applied in the simulation setup is referred from the experimental and numerical study of Kim et al. (2009) and Abdelmohimen et al. (n.d.) respectively. The Reynolds number of air flow at the inlet is set to 1333, 2667, 4000 and 5334 at 25 ℃, and with an inlet condition of inlet hydraulic diameter and turbulence intensity of 5%, the corresponding flow rate is calculated with Equation (3.6) and tabulated in Table 3.2, while the inlet hydraulic diameter is calculated with Equation (3.7). In this study, the heat sink is subjected to impinging air flow, where the air flows